 CMES, vol.66, no.2, pp.101-116, 2010

Dynamic Stress around Two Cylindrical Inclusions in Functionally Graded Materials under Non-Homogeneous Shear Waves

Xue-Qian Fang[1], Jin-Xi Liu[1], Ming-Zhang Chen[1] and Li-Yong Fu[1]

Abstract: In the authors' previous work (Zhang et al., 2010), the dynamic stress resulting from two cavities in exponential functional graded materials subjected to non-homogeneous shear waves has been studied. In this paper, the wave function expansion method is further developed to the case of two cylindrical inclusions embedded in functional graded materials, and the incident angle is also considered. The multiple scattering and refraction of non-homogeneous shear waves around the two inclusions are described accurately. The dynamic stress concentration factors around the two inclusions are presented analytically and numerically. The multiple effects of geometrical and physical parameters on the dynamic stress in functional graded materials are analyzed. These results can provide important reference in predicting the dynamic response of functional graded materials.

Keywords: Functionally graded materials; Non-homogeneous shear waves; Wave function expansion method; Two inclusions

1 Introduction

As a new type of non-homogeneous materials, functionally graded materials (FGMs) have found broad applications in high-temperature environments such as space shuttle, advanced turbine systems, aircraft engines, pressure vessels and combustion chambers. Over the past decades, theoretical and experimental investigations on FGMs have received considerable attention.

To increase the stability during the serving, it is important to understand the strength properties of FGMs subjected to various loading. In FGMs, the embedded discontinuities, such as cavities, cracks and inclusions are the major reason of reducing the strength of FGMs. Therefore, the study on the response of FGMs with discontinuities is attracting much interests in recent years. In the past decade, a considerable

[1] Department of Engineering Mechanics, Shijiazhuang Tiedao University, Shijiazhuang 050043,P.R. China

amount of research work has concentrated on the fracture mechanics in FGMs under the static loadings (Wang et al., 2003; Sladek et al., 2005; Zhou et al., 2009).

Most recently, due to the practical significance of dynamic case, the investigations on the deformation and fracture in FGMs under dynamic loading are becoming more important. Recently, Li and Weng (2001) presented the dynamic stress intensity factor of a cylindrical interface crack located between two coaxial dissimilar homogeneous cylinders that were bonded with a functionally graded interlayer and subjected to a torsion impact loading. Chen and Liu (2005) studied the transient response of an embedded crack and edge crack perpendicular to the boundary of an orthotropic functionally graded strip. Ma et al. (2007) investigated the dynamic behavior of a finite crack in functionally graded materials subjected to the normally incident elastic harmonic waves.

To predict the dynamic response of FGMs under various loadings, the study on the wave scattering in FGMs is very important. However, the propagation and and scattering of elastic waves from discontinuities (e.g., cavities, inclusions and cracks) in FGMs are quite different from those in common materials. In FGMs, the non-homogeneous elastic waves come into being. In our previous work, the scattering of a circular cavity buried in semi-infinite FGMs (Fang et al. 2007a) and a semi-infinite slab of FGMs (Fang et al. 2007b) have been studied. Most recently, the multiple scattering effects of non-homogeneous waves from two cavities have been studied (Zhang et al., 2010). In this paper, this work is extended to the case of two cylindrical inclusions in exponential functionally graded materials subjected to the oblique incident wave, and the refracted waves in the cylindrical inclusions are described accurately.

The remainder of this paper is organized as follows: Section 2 describes the problem, and the general solution of this problem is obtained. In Section 3, the incident, scattering and refracting waves in FGMs are described by using wave function expansion method. Boundary conditions around the two inclusions are presented in Section 4. In Section 5, the expanded mode coefficients are determined by satisfying the boundary conditions. Numerical examples are given in Section 6, and the effects of the geometric and material parameters on the dynamic stress concentration factors around the inclusions are analyzed. In Section 7, conclusion of this study is presented.

2 Problem description and governing equation

An infinite functionally graded material embedded with two cylindrical inclusions is considered, as depicted in Fig.1. The relative position of the two inclusions is shown in Fig.1. The radii of the two cylindrical inclusions are denoted as a_1 and

a_2. The distance between the two centers of the two inclusions is b. To describe the wave fields in FGMs, three Cartesian coordinate systems are set up. Suppose that an anti-plane shear wave with frequency ω propagates along the positive x direction in FGMs, and the incident angle is θ_0.

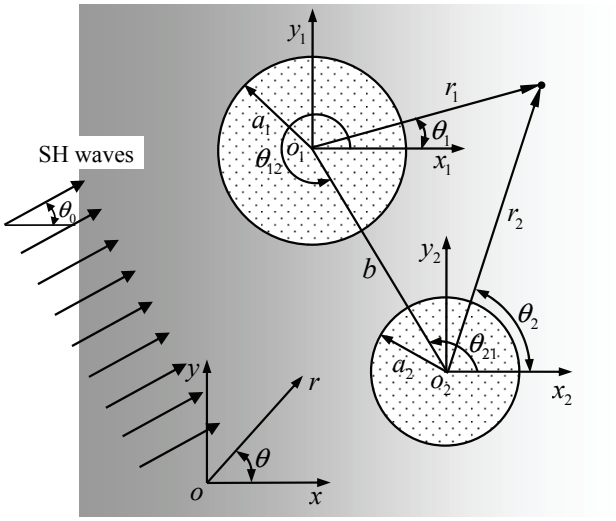

Figure 1: Schematic of two inclusions and the incident shear waves in functionally graded materials

The shear modulus and mass density of the two inclusions are denoted by μ_c and ρ_c. The gradient direction of FGMs is along the x-axis. Since the effect of Poisson's ratio on the dynamic stress is negligible, the Poisson's ratio is assumed to be a constant. It is assumed that the shear modulus and density of materials vary continuously, and they dependent only on the x coordinate. They are modeled by an exponential function, i.e.,

$$\mu(x) = \mu_0 e^{2\beta x}, \quad \rho(x) = \rho_0 e^{2\beta x}, \tag{1}$$

where μ_0 and ρ_0 are the shear modulus and density of materials at the position of $x = 0$, respectively, and β is a non-homogeneous parameter which denotes the exponent of spatial variation of the shear modulus and density of materials. It is noted that this assumption is very common in many other papers (Wang et al., 2003; Ma et al., 2007).

In the case of this paper, only the anti-plane displacement in FGMs is considered. In our previous work (Zhang et al. 2010), it has been found that the general solution

of the scattered field resulting from the inclusions in FGMs can be described as

$$u^{(s)} = e^{-\beta r\cos\theta}\sum_{n=-\infty}^{\infty} a_n H_n^{(1)}(\kappa r)e^{in\theta_1}e^{-i\omega t}, \tag{2}$$

where $H_n^{(1)}(\cdot)$ is the nth Hankel function of the first kind, a_n are the mode coefficients of the scattered waves, and determined by satisfying the boundary conditions. The propagating wave number κ is expressed as

$$\kappa = (k_s^2 - \beta^2)^{1/2}, \tag{3}$$

where $k_s = \omega/c_s$ is the wave number of elastic waves, and $c_s = \sqrt{\mu_0/\rho_0}$. The solution of the scattered-reflected waves is similar as that of the scattered waves.

3 The multiple scattering of elastic waves from the two inclusions

Consider an anti-plane shear wave propagating along the positive x direction with an incident angle θ_0. Following the work of Pao and Mao (1973), the wave fields in FGMs can be expressed as follows.

a. Incident wave fields in the two local coordinate systems

In the local cylindrical coordinate systems (r_1,θ_1) and (r_2,θ_2) of the two inclusions, the incident waves can be described as

$$u_1^{(in)} = u_0 e^{-\beta r_1\cos\theta_1}\sum_{n=-\infty}^{\infty} i^n J_n(\kappa r_1)e^{in(\theta_1-\theta_0)}e^{-i\omega t}, \tag{4}$$

$$u_2^{(in)} = u_0 e^{-\beta(r_2\cos\theta_2 + b\cos\theta_{12})}\sum_{n=-\infty}^{\infty} i^n J_n(\kappa r_2)e^{in(\theta_2-\theta_0)}e^{-i\omega t}, \tag{5}$$

where w_0 is amplitude of incident waves, κ is the wave number of propagating waves, $J_n(\cdot)$is nth Bessel function of first kind. For convenience, the time factor is omitted in the following notations.

b. Scattered wave fields in the two local coordinate systems

When the non-homogeneous shear wave propagates in FGMs, it is scattered by the two inclusions at first. The non-homogeneous scattered wave from one inclusion is scattered by another inclusion again, and the multiple scattering of non-homogeneous waves between the two inclusions arises. This complex phenomenon is shown in Fig.1.

In the two local cylindrical coordinate systems, the scattered fields resulting from the two inclusions in FGMs can be described as

$$u_1^{(s)} = u_0 e^{-\beta r_1\cos\theta_1}\sum_{n=-\infty}^{\infty} A_n H_n^{(1)}(\kappa r_1)e^{in\theta_1}, \tag{6}$$

$$u_2^{(s)} = u_0 e^{-\beta r_2 \cos\theta_2} \sum_{n=-\infty}^{\infty} B_n H_n^{(1)}(\kappa r_2) e^{in\theta_2}, \tag{7}$$

where $r_1 = (x_1, y_1)$, $r_2 = (x_2, y_2)$, and A_n and B_n are the mode coefficients of the scattered waves.

Thus, the total fields of elastic waves in FGMs are taken to be the superposition of the incident field, the scattered fields resulting from the two cylindrical inclusions, namely,

$$u_1^{(t)} = u_1^{(in)} + u_1^{(s)} + u_2^{(s)}, \tag{8}$$

$$u_2^{(t)} = u_2^{(in)} + u_2^{(s)} + u_1^{(s)}. \tag{9}$$

c. Refracted wave fields in the two local coordinate systems

The refracted waves, being confined inside the cylindrical inhomogeneityinclusion, are standing waves, and represented by

$$u_1^{(r)} = u_0 \sum_{n=-\infty}^{\infty} C_n J_n(k_c r_1) e^{in\theta_1}, \tag{10}$$

$$u_2^{(r)} = u_0 \sum_{n=-\infty}^{\infty} D_n J_n(k_c r_2) e^{in\theta_2}, \tag{11}$$

where the cylindrical Bessel functions of the first kind are used to obtain the standing waves, C_n and D_n are the refracted mode coefficients, and $k_c = \omega/c_c$ with $c_c = \sqrt{\mu_c/\rho_c}$. It should be noted that the refracted waves only exist inside the cylindrical inclusion, and do not influence the wave fields outside the cylindrical inclusion.

4 Boundary conditions around the two inclusions

The boundary conditions around the two inclusions are that the displacement field and radial shear stress are continuous. They can be expressed as

$$u_i^{(t)} = u_i^{(r)}, \quad i = 1, 2, \tag{12}$$

$$\mu(r_i, \theta_i) \frac{\partial u_i^{(t)}}{\partial r_i} = \mu_c \frac{\partial u_i^{(r)}}{\partial r_i}, \quad i = 1, 2. \tag{13}$$

5 Determination of mode coefficients and dynamic stress concentration factor

By satisfying the boundary conditions around the two inclusions, the scattering and refracting mode coefficients of elastic waves are determined.

To accomplish the superposition of wave field in the two local coordinate system (r_i, θ_i), the addition theorem for Bessel function is used, i.e.,

$$H_n^{(1)}(\kappa r_2)e^{in\theta_2} = \sum_{m=-\infty}^{\infty} e^{i(m-n)\theta_{21}} H_{m-n}^{(1)}(\kappa b) J_m(\kappa r_1) e^{im\theta_1}, \tag{14}$$

$$H_n^{(1)}(\kappa r_1)e^{in\theta_1} = \sum_{m=-\infty}^{\infty} e^{i(m-n)\theta_{12}} H_{m-n}^{(1)}(\kappa b) J_m(\kappa r_2) e^{im\theta_2}, \tag{15}$$

It is noted that θ_{21}, θ_{12} and b are shown in Fig.1.

So, the following translation relations of coordinate systems can be obtained

$$e^{-\beta r_2 \cos\theta_2} \sum_{n=-\infty}^{\infty} H_n^{(1)}(\kappa r_2) e^{in\theta_2} = e^{-\beta(r_1\cos\theta_1 + b\cos\theta_{21})} \sum_{n=-\infty}^{\infty} \sum_{m=-\infty}^{\infty} e^{i(m-n)\theta_{21}} H_{m-n}^{(1)}(\kappa b) J_m(\kappa r_1) e^{im\theta_1}, \tag{16}$$

$$e^{-\beta r_1 \cos\theta_1} \sum_{n=-\infty}^{\infty} H_n^{(1)}(\kappa r_1) e^{in\theta_1} = e^{-\beta(r_2\cos\theta_2 + b\cos\theta_{12})} \sum_{n=-\infty}^{\infty} \sum_{m=-\infty}^{\infty} e^{i(m-n)\theta_{12}} H_{m-n}^{(1)}(\kappa b) J_m(\kappa r_2) e^{im\theta_2}, \tag{17}$$

where

$$r_2 = \sqrt{r_1^2 + b^2 - 2r_1 b\cos(\pi - \theta_{21} + \theta_1)},$$

and

$$r_1 = \sqrt{r_2^2 + b^2 - 2r_2 b\cos(\pi - \theta_{12} + \theta_2)}.$$

Substituting Eqs.(8)-(11) into Eqs.(12)-(13), and using the orthogonal relation of $e^{-is\theta}$, one can obtain a set of linear algebra equations determining the mode coefficients A_n, B_n, C_n and D_n.

When time factor is omitted, the relations among every mode coefficient of scattered waves can be written as

$$A_s e^{-\beta a_1 \cos\theta_1} H_n^{(1)}(\kappa a_1) + e^{-\beta(a_1\cos\theta_1 + b\cos\theta_{21})} \sum_{n=-\infty}^{\infty} B_n e^{\mathrm{i}(s-n)\theta_{21}} H_{s-n}^{(1)}(\kappa b) J_s(\kappa a_1) - C_n J_n(k_c a_1) = -\mathrm{i}^s e^{-\beta a_1 \cos\theta_1} J_s(\kappa a_1) e^{-\mathrm{i}n\theta_0}, \quad (18)$$

$$e^{-\beta(a_2\cos\theta_2 + b\cos\theta_{12})} \sum_{n=-\infty}^{\infty} A_n e^{\mathrm{i}(s-n)\theta_{12}} H_{s-n}^{(1)}(\kappa b) J_s(\kappa a_2) + e^{-\beta a_2\cos\theta_2} B_s H_s^{(1)}(\kappa a_2) - D_s J_s(k_c a_2) = -\mathrm{i}^s e^{-\beta(a_2\cos\theta_2 + b\cos\theta_{12})} J_s(\kappa a_2) e^{-\mathrm{i}n\theta_0}, \quad (19)$$

$$\begin{aligned} &A_s e^{\beta a_1\cos\theta_1} \left\{ -\beta\cos\theta_1 H_s^{(1)}(\kappa a_1) + \frac{1}{a_1}\left[s H_s^{(1)}(\kappa a_1) - \kappa a_1 H_{s+1}^{(1)}(\kappa a_1)\right]\right\} \\ &+ e^{\beta(a_1\cos\theta_1 - b\cos\theta_{21})} \sum_{n=-\infty}^{\infty} B_n e^{\mathrm{i}(s-n)\theta_{21}} H_{s-n}^{(1)}(\kappa b) \\ &\left\{ -\beta\cos\theta_1 J_s(\kappa a_1) + \frac{1}{a_1}\left[s J_s(\kappa a_1) - \kappa a_1 J_{s+1}(\kappa a_1)\right]\right\} \\ &- C_n \frac{\mu_c}{\mu_0}\frac{1}{a_1}\left[s J_s(k_c a_1) - k_c a_1 J_{s+1}(k_c a_1)\right] \\ &\quad = \mathrm{i}^s e^{\beta a_1\cos\theta_1}\left\{ \beta\cos\theta_1 J_s(\kappa a_1) - \frac{1}{a_1}\left[s J_s(\kappa a_1) - \kappa a_1 J_{s+1}(\kappa a_1)\right]\right\} e^{-\mathrm{i}n\theta_0}, \end{aligned} \quad (20)$$

$$\begin{aligned} &e^{\beta(a_2\cos\theta_2 - b\cos\theta_{12})} \sum_{n=-\infty}^{\infty} A_n e^{\mathrm{i}(s-n)\theta_{12}} H_{s-n}^{(1)}(\kappa b) \\ &\left\{ -\beta\cos\theta_2 J_s(\kappa a_2) + \frac{1}{a_2}\left[s J_s(\kappa a_2) - \kappa a_2 J_{s+1}(\kappa a_2)\right]\right\} \\ &+ e^{\beta a_2\cos\theta_2} B_s \left\{ -\beta\cos\theta_2 H_s^{(1)}(\kappa a_2) + \frac{1}{a_2}\left[s H_s^{(1)}(\kappa a_2) - \kappa a_2 H_{s+1}^{(1)}(\kappa a_2)\right]\right\} \\ &- D_s \frac{\mu_c}{\mu_0}\frac{1}{a_2}\left[s J_s(\kappa_c a_2) - \kappa_c a_2 J_{s+1}(\kappa_c a_2)\right] \\ &= \mathrm{i}^s e^{\beta(a_2\cos\theta_2 + b\cos\theta_{12})}\left\{ \beta\cos\theta_2 J_s(\kappa a_2) - \frac{1}{a_2}\left[s J_s(\kappa a_2) - \kappa a_2 J_{s+1}(\kappa a_2)\right]\right\} e^{-\mathrm{i}n\theta_0}, \end{aligned} \quad (21)$$

After rearrangement of Eqs.(18)-(21), the following matrix equation can be obtained

$$[E]_s\{X_s\}_s = \{A\}_s, \quad s = 0, \pm 1, \pm 2, \ldots \infty, \quad (22)$$

The mode coefficients can be obtained by solving Eq.(22).

Dynamic stress concentration is an important factor influencing the strength of FGMs. According to the definition of the dynamic stress concentration factor(*DSCF*) [10], the *DSCF* is the ratio of the circumferential shear stress around the inclusions to the maximum stress. Thus, the *DSCF* around the cylindrical inclusions in FGMs is expressed as

$$DSCF = \tau^*_{\theta z} = |\tau_{\theta z}/\tau_0|, \tag{23}$$

where $\tau_{\theta z} = \mu \frac{\partial u}{\partial \theta}$, and $\tau_0 = \mu\mu_0\kappa$.

Thus, the *DSCF* around the two inclusions can be written as

$$\begin{aligned}\tau^{*(1)}_{\theta z} &= \frac{1}{\kappa a_1} e^{-\beta a_1 \cos\theta_1} \sum_{n=-\infty}^{\infty} \mathrm{i}^n (\beta a_1 \sin\theta_1 + \mathrm{i}n) J_n(\kappa a_1) e^{\mathrm{i}n\theta_1} e^{-\mathrm{i}n\theta_0} \\ &+ \frac{1}{\kappa a_1} e^{-\beta a_1 \cos\theta_1} \sum_{n=-\infty}^{\infty} A_n (\beta a_1 \sin\theta_1 + \mathrm{i}n) H^{(1)}_n(\kappa a_1) e^{\mathrm{i}n\theta_1} \\ &+ \frac{1}{\kappa a_1} e^{-\beta(a_1\cos\theta_1 + b\cos\theta_{21})} \\ &\qquad \sum_{n=-\infty}^{\infty}\sum_{m=-\infty}^{\infty} B_n e^{\mathrm{i}(m-n)\theta_{21}} H^{(1)}_{m-n}(\kappa b) (\beta a_1 \sin\theta_1 + \mathrm{i}m) J_m(\kappa a_1) e^{\mathrm{i}m\theta_1}, \end{aligned} \tag{24}$$

$$\begin{aligned}\tau^{*(2)}_{\theta z} &= \frac{1}{\kappa a_2} e^{-\beta a_2 \cos\theta_2} \sum_{n=-\infty}^{\infty} \mathrm{i}^n (\beta a_2 \sin\theta_2 + \mathrm{i}n) J_n(\kappa a_2) e^{\mathrm{i}n\theta_2} e^{-\mathrm{i}n\theta_0} \\ &+ \frac{1}{\kappa a_2} e^{-\beta a_2 \cos\theta_2} \sum_{n=-\infty}^{\infty} B_n (\beta a_2 \sin\theta_2 + \mathrm{i}n) H^{(1)}_n(\kappa a_2) e^{\mathrm{i}n\theta_2} \\ &+ \frac{1}{\kappa a_2} e^{-\beta(a_2\cos\theta_2 + b\cos\theta_{12})} \\ &\qquad \sum_{n=-\infty}^{\infty}\sum_{m=-\infty}^{\infty} A_n e^{\mathrm{i}(m-n)\theta_{12}} H^{(1)}_{m-n}(\kappa b) (\beta a_2 \sin\theta_2 + \mathrm{i}m) J_m(\kappa a_2) e^{\mathrm{i}m\theta_2}. \end{aligned} \tag{25}$$

6 Numerical examples and analysis

To analyze the effects of physical and geometrical parameters of FGMs on the the dynamic stress in the structure, the following numerical solutions are presented. For convenience, it is assumed that the two inclusions have the same radius, i.e., $a_1 = a_2 = a$.

In the following, a characteristic length a, where a is the radius of the two inclusions is introduced. Other dimensionless variables and quantities have been chosen for

computation: the incident wave number is $k^* = ka = 0.1 - 3.0$, the material properties ratios of the inclusion to matrix are $\mu^* = \mu_c/\mu_0 = 0.1 - 4.0$, $\rho^* = \rho_c/\rho_0 = 0.1 - 2.0$, the non-homogeneous parameter of FGMs is $\beta^* = \beta a = -0.5 - 0.5$, and the distance between the two inclusions is $b^* = b/a = 2.1 - 8.0$.

The reduced case of the present dynamic model is computed in Fig.2. In Fig.2, the dynamic stresses around the inclusion 1 are illustrated with parameters: $k^* = 0.5$, $b^* = 10.0$, $\mu^* = 0$,$\theta_{21} = \pi/2$, and $\theta_0 = 0$. When$\beta = 0$, the functionally graded material is reduced to homogeneous material. When the distance between the two inclusions is $b^* = 10.0$, the interaction between the two inclusions vanishes. From Fig.2, it is clear that the dynamic stress is symmetrical about the two axes, and the maximum dynamic stress occurs at the position of $\theta_1 = \pm\pi/2$. The maximum *DSCF* is about 2.0. These conclusions are consistent with those in Pao and Mow (1973) and Zhang et al. (2001). When the distance between the two inclusions becomes small, the dynamic stress at the positions near the inclusion 2 increases greatly. However, the variation of the dynamic stress at the positions far from the inclusion 2 is very little. The phenomenon is due to the multiple scattering of shear waves between the two inclusions. When the distance between the two inclusions is little, the multiple scattering effects are very strong, and so the dynamic stress increases greatly.

Fig.3 shows the *DSCF*s around the inclusion 1 with different non-homogeneous pa-

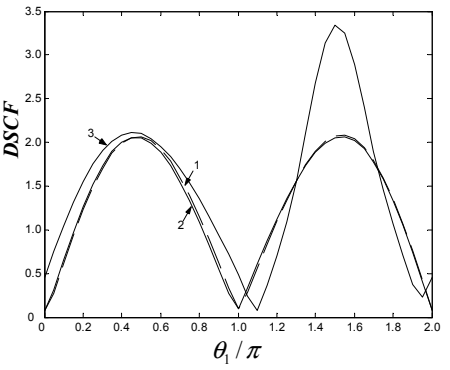

Figure 2: Comparison with the existing solutions with $k^* = 0.5, \mu^* = 0, \beta = 0, \theta_{21} = \pi/2, \theta_0 = 0$. 1. $b^* = 10.0$ obtained from this paper; 2. $b^* = 10.0$ obtained from Pao and Mow (1973); 3. $b^* = 2.5$

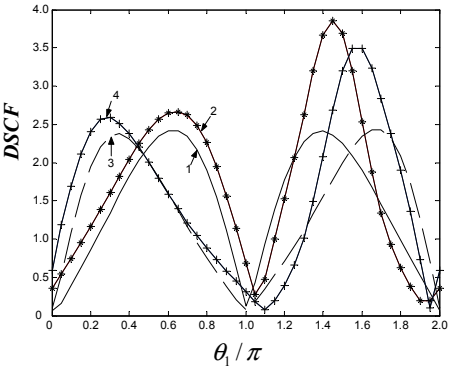

Figure 3: Dynamic stress concentration factor around the inclusion 1 with $k^* = 0.5, \mu^* = 0, \theta_{21} = \pi/2, \theta_0 = 0$. 1. $\beta = 0.2, b^* = 8.0$; 2. $\beta = 0.2, b^* = 2.5$; 3. $\beta = -0.2, b^* = 8.0$; 4. $\beta = -0.2, b^* = 2.5$

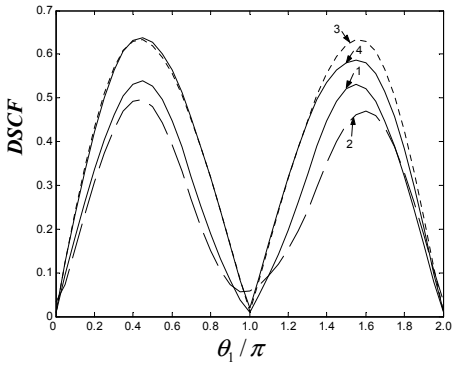

Figure 4: Dynamic stress concentration factor around the inclusion 1 with $k^* = 0.5, \mu^* = 4.0, \rho^* = 2.0, \theta_{21} = \pi/2, \theta_0 =$ 0. 1. $\beta = 0.2, b^* = 8.0$; 2. $\beta = 0.2, b^* = 2.5$; 3. $\beta = -0.2, b^* = 8.0$; 4. $\beta = -0.2, b^* = 2.5$

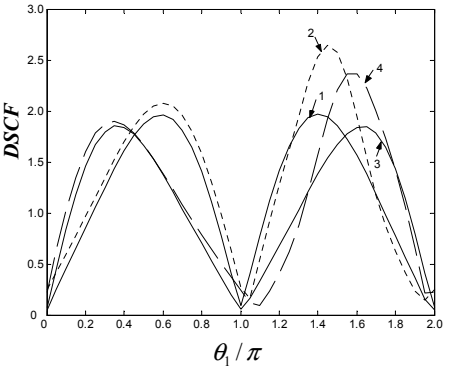

Figure 5: Dynamic stress concentration factor around the inclusion 1 with $k^* = 0.5, \mu^* = 0.2, \rho^* = 0.1, \theta_{21} = \pi/2, \theta_0 =$ 0. 1. $\beta = 0.2, b^* = 8.0$; 2. $\beta = 0.2, b^* = 2.5$; 3. $\beta = -0.2, b^* = 8.0$; 4. $\beta = -0.2, b^* = 2.5$

rameters. It can be seen that the non-homogeneous property expresses great effect on the dynamic stress distribution around the inclusion. The maximum dynamic stress increases with the absolute value of non-homogeneous parameter. Comparing with the results in Fig.2, it is clear that the distance between the two inclusions expresses great effect on the dynamic stress around the inclusion when the non-homogeneous property is considered. If the distance between the two inclusions is little, the dynamic stress around the inclusion increases. However, the variation of the dynamic stress at the positions near $\theta_1 = \pi/2, 3\pi/2$ is the greatest. If the non-homogeneous parameter is great than zero, that is to say, the material properties increase in the positive *x*direction, the effect of the distance between the two inclusions is greater.

Fig.4 shows the *DSCF*s around the inclusion 1 with different non-homogeneous parameters when the inclusions are stiffer that the matrix. Comparing with the results in Fig.3, it can be seen that the existence of the stiffer inclusion expresses great effect on the dynamic stress. In this case, the effect of the distance between the two inclusion decreases. This phenomen results from the refraction of shear waves around the stiffer inclusion. The refraction effect increases with the value of μ^*. Different from the case of cavities, the dynamic stress decreases if the distance between the two inclusions is little.

Fig.5 displays the *DSCF*s around the inclusion 1 with different non-homogeneous

parameters when the inclusions are softer that the matrix. It can be seen that the effect of the inclusion on the dynamic stress is quite different from that in Fig.4. If the inclusion is softer, the effects of the non-homogeneous parameter and the distance between the two inclusions are great. If the non-homogeneous is greater than zero, that is to say, the material properties increase in the x direction, the maximum dynamic stress around the inclusions has a trend of shifting towards the illuminate side of the inclusion. However, the maximum dynamic stress around the inclusions has a trend of shifting towards the shadow side of the inclusion if the non-homogeneous is less than zero. The dynamic stresses at the positions near the second inclusion increase greatly if the distance between the two inclusion is little. The greater the non-homogeneous parameter, the greater the effect of the distance between the two inclusion.

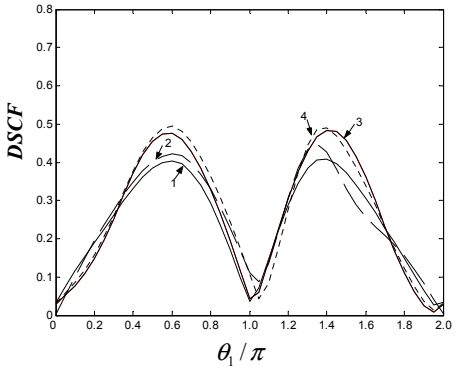

Figure 6: Dynamic stress concentration factor around the inclusion 1 with $k^* = 1.5, \mu^* = 4.0, \rho^* = 2.0, \theta_{21} = \pi/2, \theta_0 =$ 0. 1. $\beta = 0.2, b^* = 8.0$; 2. $\beta = 0.2, b^* =$ 2.5; 3. $\beta = -0.2, b^* = 8.0$; 4. $\beta =$ $-0.2, b^* = 2.5$

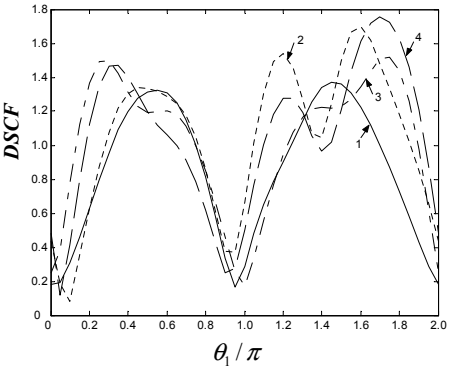

Figure 7: Dynamic stress concentration factor around the inclusion 1 with $k^* = 1.5, \mu^* = 0.2, \rho^* = 0.1, \theta_{21} = \pi/2, \theta_0 =$ 0. 1. $\beta = 0.2, b^* = 8.0$; 2. $\beta = 0.2, b^* =$ 2.5; 3. $\beta = -0.2, b^* = 8.0$; 4. $\beta =$ $-0.2, b^* = 2.5$

Fig.6 displays the *DSCF*s around the stiffer cylindrical inclusion 1 with different non-homogeneous parameters in the region of high frequency. Comparing with the results in Fig.4, it can be seen that the dynamic stress around the inclusion decreases if the wave frequency is high. It is due to the strong refraction of waves around the stiffer inclusion in the region of high frequency. It is also clear that the effects of non-homogeneous parameter and the distance between the two inclusions decrease. If the non-homogeneous parameter is less than zero, the effect of the distance between the two inclusions is even less.

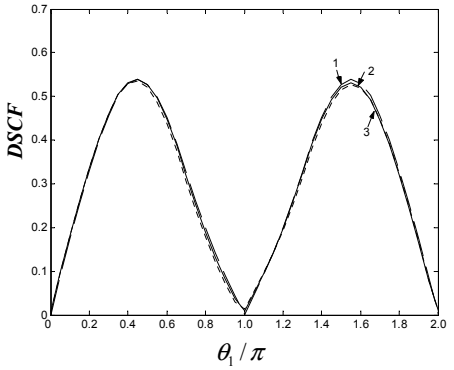

Figure 8: Dynamic stress concentration factor around the inclusion 1 with $k^* = 0.5, \mu^* = 4.0, \rho^* = 2.0, \beta = 0.2, b^* = 8.0, \theta_0 = 0$. 1. $\theta_{21} = \pi/4$; 2. $\theta_{21} = \pi/2$; 3. $\theta_{21} = 3\pi/2$

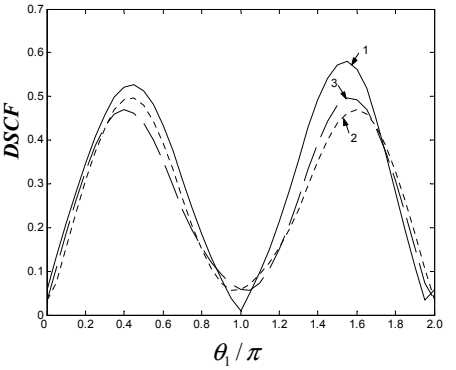

Figure 9: Dynamic stress concentration factor around the inclusion 1 with $k^* = 0.5, \mu^* = 4.0, \rho^* = 2.0, \beta = 0.2, b^* = 2.5, \theta_0 = 0$. 1. $\theta_{21} = \pi/4$; 2. $\theta_{21} = \pi/2$; 3. $\theta_{21} = 3\pi/2$

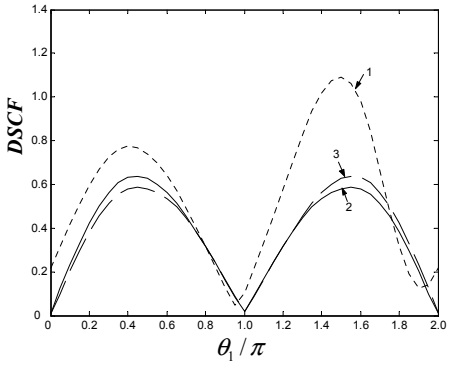

Figure 10: Dynamic stress concentration factor around the inclusion 1 with $k^* = 0.5, \mu^* = 4.0, \rho^* = 2.0, \beta = -0.2, b^* = 2.5, \theta_0 = 0$. 1. $\theta_{21} = \pi/4$; 2. $\theta_{21} = \pi/2$; 3. $\theta_{21} = 3\pi/2$

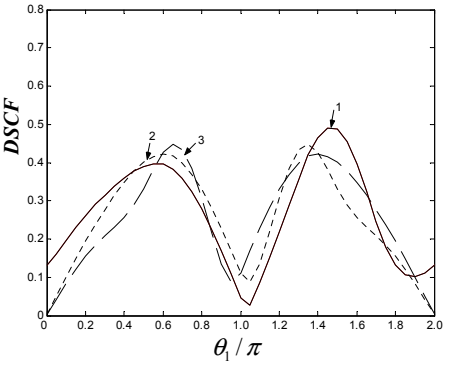

Figure 11: Dynamic stress concentration factor around the inclusion 1 with $k^* = 1.5, \mu^* = 4.0, \rho^* = 2.0, \beta = 0.2, b^* = 2.5, \theta_0 = 0$. 1. $\theta_{21} = \pi/4$; 2. $\theta_{21} = \pi/2$; 3. $\theta_{21} = 3\pi/2$

Fig.7 displays the *DSCF*s around the softer cylindrical inclusion 1 with different non-homogeneous parameters in the region of high frequency. It can be seen that the effect of wave frequency on the dynamic stress is great if the inclusion is soft. Comparing with the results in Fig.6, it is clear that the effect of non-homogeneous

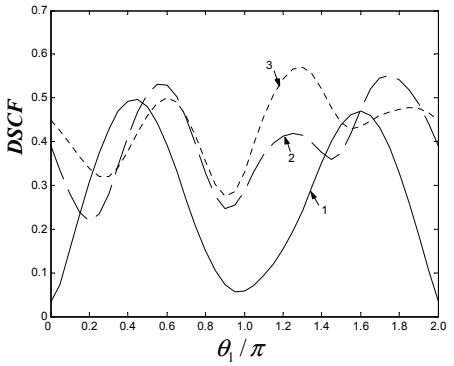

Figure 12: Dynamic stress concentration factor around the inclusion 1 with $k^* = 0.5, \mu^* = 4.0, \rho^* = 2.0, \beta = 0.2, b^* = 2.5, \theta_{21} = \pi/2$. 1. $\theta_0 = 0$; 2. $\theta_0 = \pi/3$; 3. $\theta_0 = \pi/2$

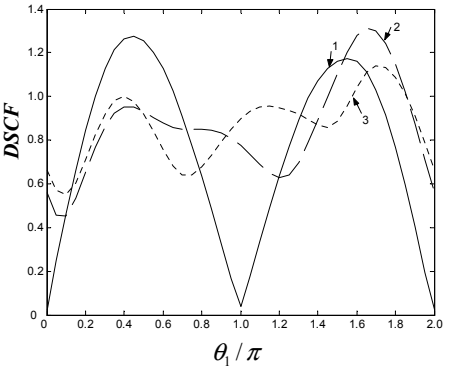

Figure 13: Dynamic stress concentration factor around the inclusion 1 with $k^* = 0.5, \mu^* = 4.0, \rho^* = 2.0, \beta = -0.2, b^* = 2.5, \theta_{21} = \pi/2$. 1. $\theta_0 = 0$; 2. $\theta_0 = \pi/3$; 3. $\theta_0 = \pi/2$

parameter on the dynamic stress increases due to the existenc of softer inclusion. However, the effect of the distance between the two inclusions decreases.

To find the effect of the relative position of the two inclusions on the dynamic stress, Figs.8-11 are plotted. In Figs.8-10, the wave frequency is low. In Fig.11, the wave frequency is high.

In Fig.8, the inclusion is stiffer, the non-homogeneous parameter is greater than zero, and the interactive effect of the two inclusions disappears. It is clear that the relative position of the two inclusions nearly expresses no effect on the the dynamic stress.

In Fig.9, the distance between the two inclusions is very little. It can be seen that the effect of the relative position of the two inclusions becomes great. At the positions near $\theta_1 = \pi/2$, the dynamic stress decreases with the increase of θ_{21}. However, at the positions near $\theta_1 = 3\pi/2$, the dynamic stress in the case of $\theta_{21} = \pi/2$ is the minimum.

In Fig.10, the distance between the two inclusions is very little, and the non-homogeneous parameter is less than zero. Comparing with the results in Fig.9, it can be seen that the relative position of the two inclusions shows great effect on the dynamic stress, expecially at the positions near the second inclusion. With the variation of θ_{21}, the distribution of the maximum dynamic stress around the inclusion has a great variation.

In Fig.9, it can be seen that the effect of the relative position of the two inclusions on the dynamic stress is great only at the positions near $\theta_{21} = \pi/2, 3\pi/2$. In Fig.11. the wave frequency is high. It is cleat that the effect at other positions also shows great variation. When the value of θ_{21} is little, the effect of the distance between the two inclusions becomes great.

Figs.12-13 illustrate the effect of incident angle on the *DSCF*s around the inclusion 1. It can be seen that more peaks occur if the incident angle increases. The variation of dynamic stress around the inclusion decreases with the increase of incident angle. The greater the incident angle, the less the variation of the dynamic stress around the inclusion. If the wave frequench is high, the effect of the incident angle on the dynamic stress increases.

7 Conclusion

In this paper, the multiple scattering of non-homogeneous shear waves from two inclusions and dynamic stress in functionally graded materials are studied. Wave function expansion method for non-homogeneous waves is used to express the wave field in FGMs. The effects of the material properties of inclusions, the relative distance and position of the two inclusions, the non-homogeneous parameters and the incident angle of wave on the dynamic stress around the inclusions are analyzed, and the interactive effects of these parameters are also presented. The main findings of this paper are as follows.

1. The non-homogeneous properties of FGMs express great effect on the dynamic stress around the inclusion. If the non-homogeneous parameter is great than zero, that is to say, the material properties increase in the positive x direction, the effect of the distance between the two inclusions is greater.

2. When the material properties increase in the positive x direction, the maximum dynamic stress has a trend of shifting toward the illuminate side of the inclusion.

3. The effect of the distance between the two inclusion becomes little if the inclusion is stiffer. If the inclusion is softer, the effects of the non-homogeneous parameter and the distance between the two inclusions are great.

4. In the region of high frequency, if the inclusion is stiffer, the effects of non-homogeneous parameter and the distance between the two inclusions decrease. If the inclusion is softer, the effect of non-homogeneous parameter on the dynamic stress increases. However, the effect of the distance between the two inclusions decreases.

5. The effect of the relative position of the two inclusions increases if the distance between the two inclusions becomes great. If the distance between the two inclusions is very little, and the non-homogeneous parameter is less than zero. the relative position of the two inclusions shows great effect on the dynamic stress, expecially at the positions near the second inclusion.

6. The variation of dynamic stress around the inclusion decreases with the increase of incident angle. The greater the incident angle, the less the variation of the dynamic stress around the inclusion.

Acknowledgement: The paper is supported by the National Natural Science Foundation of China (Foundation No. 10972147), the Natural Science Foundation of Hebei Province, China (Foundation No. A2010001052), and the Program for Changjiang Scholars and Innovative Research Team in University.

References

Chen, J.; Liu, Z. (2005): Transient response of a mode III crack in an orthotropic functionally graded strip. *European Journal of Mechanics - A/Solids*, vol. 24, pp. 325-336.

Fang, X. Q.; Hu, C.; Du, S. Y. (2007a): Dynamic stress of a circular cavity buried in a semi-infinite functionally graded material subjected to shear waves. *ASME Journal of Applied Mechanics*, vol. 74, pp. 916-922.

Fang, X. Q.; Hu, C.; Huang, W. H. (2007b): Strain energy density of a circular cavity buried in a semi-infinite slab of functionally graded materials subjected to anti-plane shear waves. *International Journal of Solids and Structures*, vol. 44, pp. 6987-6998.

Li, C.; Weng, G. J. (2001): Dynamic stress intensity factor of a cylindrical interface crack with a functionally graded interlayer. *Mechanics of Materials*, vol. 33, pp. 325-333.

Ma, L.;, Li, J.; Abdelmoula, R.; Wu, L. Z. (2007): Dynamic stress intensity factor for cracked functionally graded orthotropic medium under time-harmonic loading. *European Journal of Mechanics -A/Solids*, vol. 26, pp.325-336.

Pao, Y. H.; Mow, C. C. (1973): *Diffraction of Elastic Waves and Dynamic Stress Concentrations*, Crane, Russak, New York.

Sladek, J.; Sladek, V.; Krivacek, J.; Zhang, C. (2005): Meshless local Petrov-Galerkin method for stress and crack analysis in 3-D axisymmetric FGM bodies. *CMES: Computer Modeling in Engineering & Sciences*, vol. 8, pp. 259-270.

Wang, B. L.; Mai, Y. W.; Sun, Y. G. (2003): Anti-plane fracture of a functionally graded material strip. *European Journal of Mechanics-A/Solids*, vol. 22, pp. 357-368.

Zhang, L. L.; Fang, X. Q; Liu, J. X.; Fu, L. Y. (2010): The multiple scattering of non-homogeneous shear waves from two cavities in functionally graded materials. *Philosophical Magazine*, vol. 90, pp.3375-3387.

Zhou, Y.T.; Li, X.; Yu, D. (2009): Transient thermal response of a partially insulated crack in an orthotropic functionally graded strip under convective heat supply. *CMES: Computer Modeling in Engineering & Sciences*, vol. 43, pp. 191-221.